Desalination and Water Treatment
www.deswater.com

doi: 10.5004/dwt.2017.20280

65 (2017) 418–427
March

Adsorption of nitrate using diatomite-supported ferric oxide nanoparticles: determination of optimum condition, kinetics, and adsorption isotherms

Saeed Dehestaniathar[a,*], Shouresh Amini[b], Afshin Maleki[a], Behzad Shahmoradi[a], Naser Reshadmanesh[a], Pari Teymouri[a]

[a]*Environmental Health Research Center, Kurdistan University of Medical Sciences, Sanandaj, Iran, Tel. +98 9127100637; Fax: +98 871 6625131; email: saeed_dehestani@yahoo.com (S. Dehestaniathar), Tel. +98 9123615550; email: maleki43@yahoo.com (A. Maleki), Tel. +98 9187705355; email: bshahmorady@gmail.com (B. Shahmoradi), Tel. +98 9188715774; email: nreshadmanesh@yahoo.com (N. Reshadmanesh), Tel. +98 9149367932; email: pari.teymouri@yahoo.com (P. Teymouri)*
[b]*Student Research Committee, Kurdistan University of Medical Sciences, Sanandaj, Iran, Tel. +98 9181841836; email: oo.shoresh@yahoo.com*

Received 11 May 2016; Accepted 22 October 2016

ABSTRACT

In the present work, nitrate adsorption onto the Fe_2O_3/diatomite was conducted in different operational parameters, such as initial nitrate concentration, amount of adsorbent, pH, and contact time. The prepared adsorbents were characterized by field emission scanning electron microscope, X-ray diffraction, Fourier transform infrared, and X-ray fluorescence spectroscopy. Kinetic and isotherm studies were also conducted. Experimental results indicated that the maximum nitrate removal could be attained at a solution pH of 4.5. For the entire adsorbent dose, the removal efficiency increased with an increase in the contact time. Furthermore, the adsorption of nitrate increased with an increase in the adsorbent concentration. The optimum Fe_2O_3/diatomite content was determined as 5 g/L. Removal amount of nitrate after 100 min was 93%, 85%, and 79% for initial nitrate concentration of 20, 60, and 100 mg/L, respectively. Pseudo-second-order and Freundlich models were the best fitted kinetic and isotherm models, respectively, for describing nitrate adsorption process.

Keywords: Nitrate; Adsorption; Fe_2O_3 nanoparticles; Diatomite; Kinetic; Isotherm

1. Introduction

The rapid population growth and industrial development have led to increase of contaminants in water bodies in many countries all around the world. One of the most important pollutants that can't be removed easily in conventional wastewater treatment plants is nutrients like nitrogen. The maximum concentration level for nitrate set by Environmental Protection Agency (EPA) and World Health Organization (WHO) is 45 and 50 mg/L NO_3^-, respectively. High concentrations of nitrogen compounds can deteriorate the aquatic environmental quality and threaten human health. It can also be harmful for aquatic environment. Therefore, there is an urgent need to develop and improve low-cost technologies for treatment of wastewater containing high concentration of nitrogen compounds. The main methods for removal of nitrate from aqueous media include physicochemical and biochemical processes. Common methods include ion exchange [1], electro deionization [2], electrodialysis [3], and reverse osmosis [4]. Adsorption is a promising method because of its simplicity and efficiency. Different kinds of adsorbents have been used for nitrate removal. The most common adsorbents include activated carbon [5], agricultural waste [6], natural clays [7], Al-MCM-41 [8], bamboo powder [9], fly ash [10], and zeolite [11]. Diatomite has recently been known as a promising adsorbent because of its unique physicochemical properties

* Corresponding author.

1944-3994/1944-3986 © 2017 Desalination Publications. All rights reserved.

such as: 80%–90% pore spaces, numerous fine microscopic pores, cavities and channels, high porosity (35%–65%), good sorption ability, low density, high permeability, high specific surface area, and active hydroxyl groups. In addition, diatomite is cheaper than activated carbon [12].

Acid treatment increases the specific surface area and adsorption capacity of diatomite [13]. It is known that iron salts play a critical role in adsorption of anions from water. Moreover, the attractive forces between the adsorbent and adsorbate depend on the modifier.

Nowadays, most of the ongoing research tries to focus on modification using nanoparticle. Among the different types of nanoparticles tested over the past decade, nanosized iron oxides have larger specific surface area, which leads to enhanced adsorption capacity [14]. Moreover, magnetic Fe_2O_3 nanoparticles can be easily separated from the water medium using a magnetic process [15].

Most of the old research has been addressed on the adsorption of anions from aqueous solution using different modified adsorbent. Modification of adsorbent is carried out to improve the capacity of adsorption process. It has been reported that modification of activated carbon enhances the removal efficiency [5]. Diatomite has been applied for the adsorption of different pollutants including dye [16], Cd [17] Pb(II) [17,18], arsenate [19], BTEX, MTBE, and TAME [13], and zinc(II) [17,20]. However, modified diatomite using Fe_2O_3 nanoparticles has not been reported as adsorbent for nitrate removal from water. The aim of this study is to investigate the performance of the modified diatomite as a low-cost bio-adsorbent for nitrate adsorption from aqueous solution. Field emission scanning electron microscope (FESEM), X-ray diffraction (XRD), X-ray fluorescence (XRF), and Fourier transform infrared (FTIR) spectroscopy were used, and point of zero charge (pH_{zpc}) was determined to characterize the sorbent surface. The effects of different parameters, including initial nitrate concentration, adsorbent dosage, pH, and contact time, on NO_3^- adsorption on the Fe_2O_3 nanoparticles were studied. Kinetic and isotherm studies were also conducted.

2. Materials and methods

2.1. Chemicals and materials

All chemicals used in present study were of analytical grade purchased from Merck except Fe_2O_3 nanoparticles, which was obtained from Nano Pars Co., Iran. Diatomite was obtained from the Bojnourd mine in Iran. The diatomite was washed with tap water to remove impurities, and then dried in an oven at 105°C for 24 h. The dried diatomite was sieved to a uniform size of 0.8–1 mm. The acid treatment of diatomite was done using 6 M H_2SO_4 under reflux conditions (at 100°C for 4 h). Hot distilled water was used for washing and rinsing until the residual acid and impurities completely removed. The coating of Fe_2O_3 nanoparticles into the pores of diatomite, using wet impregnation method (WIM), was carried out according to the protocol previously described [21]. Briefly, the required amount of commercial Fe_2O_3 nanoparticles placed into 200 mL deionized water under sonication condition in ultrasound bath for 20 min at room temperature and after that 20 g of diatomite was added to the above solution under continuous stirring for 3 h at room temperature, filtered, and dried at 105°C for 24 h. Finally, dried samples were calcined at 300°C for 3 h. Sodium nitrate was used to prepare standard stock solution of nitrate. Nitrate concentration was determined based on standard methods for the examination of water and wastewater [22]. pH adjustment to the desirable values was carried out using 0.1 M NaOH and 0.1 M HCl.

2.2. Instrumentation

In order to determine crystal structure of the adsorbents, XRD analysis was performed using Philips equipment with Cu Kα radiation at 40 kV and 30 mA in a scanning range of 5°–80° (2θ). Elemental analysis of raw diatomite was determined by XRF technique. Surface morphology of raw and modified diatomite were characterized by means of FESEM (Philips: XL 30, the Netherlands). FTIR spectroscopy (Tensor 27, Bruker, Germany) was applied to examine the chemical bounds and functional groups. The nitrate concentration was determined by a spectrophotometer (Unico-UV 2100). The pH was measured with a pH electrode Jenway part number 924 050.

2.3. Experimental procedure

In order to investigate the effect of various operational parameters (adsorbent dosage, reaction time, pH of solution, and initial nitrate concentration) on the nitrate adsorption efficiency, the batch experimental studies were carried out in 100 ml Erlenmeyer flasks. The quantity of adsorbed nitrate onto the adsorbent was determined using Eq. (1):

$$q = (C_0 - C) \times V) / m \quad (1)$$

where q, C_0, and C are the amount of adsorbed nitrate (mg g^{-1}), the initial, and final concentration of nitrate in the solution (mg L^{-1}), respectively. Moreover, V and m are volume of the solution (L) and the adsorbent weight (g), respectively.

Experimental procedure began with different pretest to determine the experimental runs and conditions. In order to determine adsorption capacity of Fe_2O_3/diatomite, experimental analyses were tested at different conditions.

The pH_{zpc} of adsorbent was determined according to the pH drift method [23]. Briefly, 0.01 M NaCl solution was made, and the pH of the solution was adjusted in the range of 2–12 using HCl or NaOH. Then, 150 mg of diatomite was added and kept for shaking for 24 h at 200 rpm at 25°C. Then, the final pH of the solution was measured, and graph was plotted between final pH and initial pH. The point where initial pH is equal to final pH has been recorded as pH_{zpc} of the diatomite.

2.4. Kinetic and isotherm studies

The adsorption kinetics of adsorption of nitrate were investigated by different models including pseudo first order, pseudo second order, Bangham, and intraparticle diffusion. Moreover, adsorption isotherms were studied using Langmuir, Freundlich, and Dubinin–Radushkevich (D–R) model. Table 1 presents the studied models for kinetic and isotherm.

Table 1
Kinetic and isotherm models used in this study

Models	Equations	Plot	Calculated coefficients	Eq. No.	Nomenclature	References
Kinetics models						
Lagergren pseudo-first-order	$\log(q_e - q_t) = \log(q_e) - K_1 - t/2.303$	$\log(q_e - q_t)$ vs. t	$q_e = 10^{\text{intercept}}$; $k_1 = -2.303 \times$ slope	(2)	q_e, equilibrium sorption capacity (mg.g^{-1}); k_1, pseudo-first-order rate constant (min^{-1})	[24]
Pseudo-second-order	$t/q_t = (1/k_2 q_e^2) + (1/q_e) \times t$	t/q_t vs. t	$q_e = 1/\text{slope}$; $k_2 = \text{slope}^2/\text{intercept}$	(3)	q_e, equilibrium sorption capacity (mg.g^{-1}); k_2, pseudo-second-order rate constant (g.mg^{-1}.min^{-1})	
Bangham	$\log(\log[C_0/(C_0 - q_t m)] = \log(k_0 m = 2{:}303\ V)) + \alpha \log t$	$\log(\log[C_0/(C_0 - q_t m)])$ vs. $\log t$	α = slope; $K_0 = 10^{\text{intercept}} \times 2.303\ V/m$	(4)	C_0, the initial metal concentration (mg.L^{-1}); m, the adsorbent mass used per liter of solution (g.L^{-1}); V, is the volume of the solution (mL); α (<1) and k_0 (mL.g^{-1}.L^{-1}), Bangham constants	
Intraparticle diffusion	$q_t = k_i t^{0.5} + C$	q_t vs. $t^{0.5}$	k_i = slope; C = intercept	(5)	k_i, the intraparticle diffusion rate constant (mg.g^{-1}.min$^{-0.5}$); C, boundary layer diffusion	
Equilibrium isotherm models						
Langmuir	$C_{eq}/q_e = 1/K_L q_m + C_{eq}/q_m$	q_e/q_e vs. q_e	K_L = slope/intercept; $q_m = 1/\text{slope}$	(6)	q_{max}, maximum sorption capacity (mg.g^{-1}); K_L, Langmuir constant (Lmg^{-1})	[25]
Freundlich	$\log q_e = \log K_f + 1/n \log C_e$	$\log q_e$ vs. $\log q_e$	$n = 1/\text{slope}$; $K_f = 10^{\text{intercept}}$	(7)	K_F, Freundlich constant (mg$^{(1-1/n)}$).L$^{1/n}$.g^{-1}); n, Freundlich exponent	
Dubinin–Radushkevich (D–R)	$\log q_e = \log q_m - \beta\varepsilon^2$	ln q_e vs. ε^2	$\varepsilon = RT \ln(1 + 1/C_e)$; $q_m = \exp(\text{intercept})$; β = slope	(8)	q_e, adsorption capacity (mol.g^{-1}); q_m, maximum adsorption capacity (mol.g^{-1}); β, the activity coefficient related to mean adsorption energy (mol^2.J^{-2}); ε, the Polanyi potential	

3. Result and discussion

3.1. Characterization of adsorbent

Fig. 1 shows the XRD pattern of raw diatomite (a) and Fe_2O_3/diatomite (b). As illustrated in this figure, cristobalite and quartz are the main crystal phases of diatomite. It can be seen that after coating of nanoparticles of Fe_2O_3 over the diatomite, the relevant hematite peaks appeared.

Elemental analysis of the row diatomite obtained by means of XRF technique is presented in Table 2. The analysis shows that SiO_2 is the main component (86%) and the metal oxides (Na_2O, Al_2O_3, P_2O_5, and Fe_2O_3) are the main minor elements.

Fig. 2 shows the FESEM photographs of raw diatomite (a, b, and c) and Fe_2O_3/diatomite (d). As shown in Fig. 2, the raw diatomite has a porous structure, while after coating, the surface of diatomite was covered by Fe_2O_3 nanoparticles.

In order to investigate how functional groups and changes in vibration of functional groups are presented on the surface of adsorbent, FTIR spectra of diatomite was examined. The identification of IR absorption bands related to vibration is given in Table 3.

The FTIR spectra of raw diatomite, Fe_2O_3/diatomite before adsorption, and Fe_2O_3/diatomite after adsorption are shown in Fig. 3 and depict the presence of various functional groups on the surface of adsorbent.

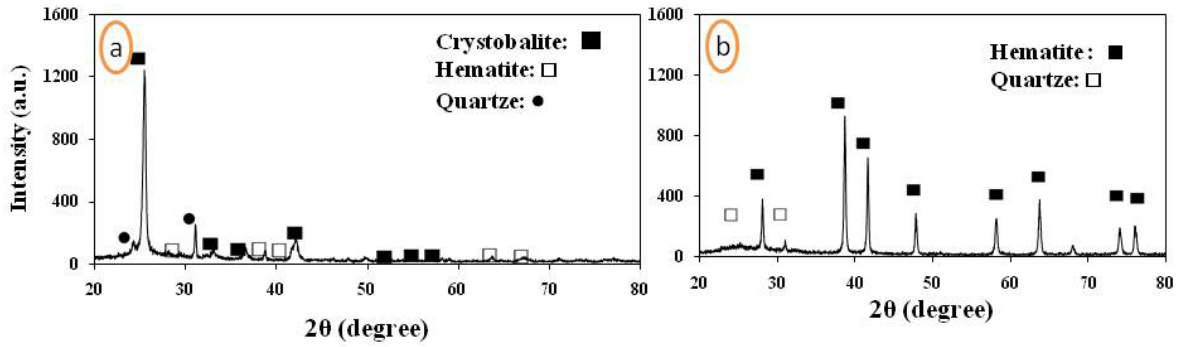

Fig. 1. XRD pattern of raw diatomite (a) and Fe_2O_3/diatomite (b).

Table 2
The elemental analysis of pure diatomite by means of XRF

Component	Content (%)
SiO_2	86
Fe_2O_3	1.37
MgO	0.25
K_2O	0.31
Al_2O_3	2.7
CaO	0.93
Na_2O	2.8
P_2O_5	1.8
TiO_2	0.8

It can be seen that there are two broad adsorption peaks at 1,633 and 3,450 cm^{-1}, which were assigned to the twisting vibration and adsorption of —OH stretching vibration, respectively [18]. The absorption peak at 1,098 cm^{-1} was due to the asymmetric stretching vibration mode of Si—O—Si bond in the diatomite [24]. The absorption peak at 798 cm^{-2} is assigned to Si—O—Al bonding that is because of impurity in the diatomite. The peak at 549 cm^{-1} was due to the Fe–OH stretching vibration. It has been shown that the peak of the α-Fe_2O_3 had higher intensity at higher pH, indicating more amount of OH^-. The additional peak at 1,119 cm^{-1} corresponded to bending modes of nitrate.

3.2. pH_{zpc}

pH_{zpc} or point of zero charge (pzc) is the pH value at which an adsorbent exhibits zero net electrical charge on the surface. When the solution pH is above the pH_{zpc}, the adsorbent surface has a negative charge, while at pH values lower than pH_{zpc}, it has a positive charge. The result of pH_{zpc} is presented in Fig. 4. As shown, the value of pH_{zpc} for diatomite is 5.6. pH_{zpc} of adsorbent (Fe_2O_3/diatomite) was found 6.1 (the data are not presented), indicating that adsorbent's surface is uncharged at solution pH of 6.1; when the solution pH is above the 6.1, the adsorbent surface has a negative charge, while at pH lower than 6.1, it has a positive charge.

3.3. Effect of pH

pH value of the solution is a critical parameter involved in the adsorption, which affects the surface chemistry of the adsorbent. The effect of solution's pH ranging from 3.5 to 9 was examined on the adsorption of nitrate. The result of experiments is presented in Fig. 5. As seen in this figure, the adsorption of nitrate onto the diatomite depends on the pH. The optimum pH at which maximum nitrate adsorption obtained was 4.5, as can be seen in Fig. 5.

3.4. Effect of Fe_2O_3/diatomite dose

In order to investigate the effect of adsorbent dose on nitrate adsorption, the adsorption process was examined in a range of 1–5 g/L. Adsorption of nitrate at different dose of Fe_2O_3/diatomite as a function of time is illustrated in Fig. 6. As shown in this figure, for the entire adsorbent dose, the removal efficiency increased with an increase in the contact time. Furthermore, the adsorption of nitrate increased with an increase in the adsorbent concentration. This can be attributed to more adsorption sites. It was found in the previous studies that difference iron content has a noticeable effect on adsorption behavior [19].

3.5. Effect of initial nitrate concentration

The adsorption of 20, 60, and 100 mg/L nitrate concentration was examined to investigate the effect of initial nitrate concentration on nitrate removal. As shown in Fig. 7, the percentage of nitrate removal was 59%, 48%, and 42% after 20 min of contact time for initial nitrate concentration of 20, 60, and 100 mg/L, respectively. Maximum adsorption of nitrate after 100 min was 93%, 85%, and 79%, respectively. Accordingly, the increase of initial nitrate concentration led to a reduction of its adsorption efficiency, which can be because of adsorption sites reduction.

3.6. Determination of equilibrium time

Variation of adsorbed nitrate as a function of contact time is illustrated in Fig. 8. As seen, adsorbed nitrate increased with an increase in time and the equilibrium reached after 150 min.

3.7. Kinetic studies

To predict batch kinetics and design an adsorption process, the rate of the adsorption reaction should be determined [25].

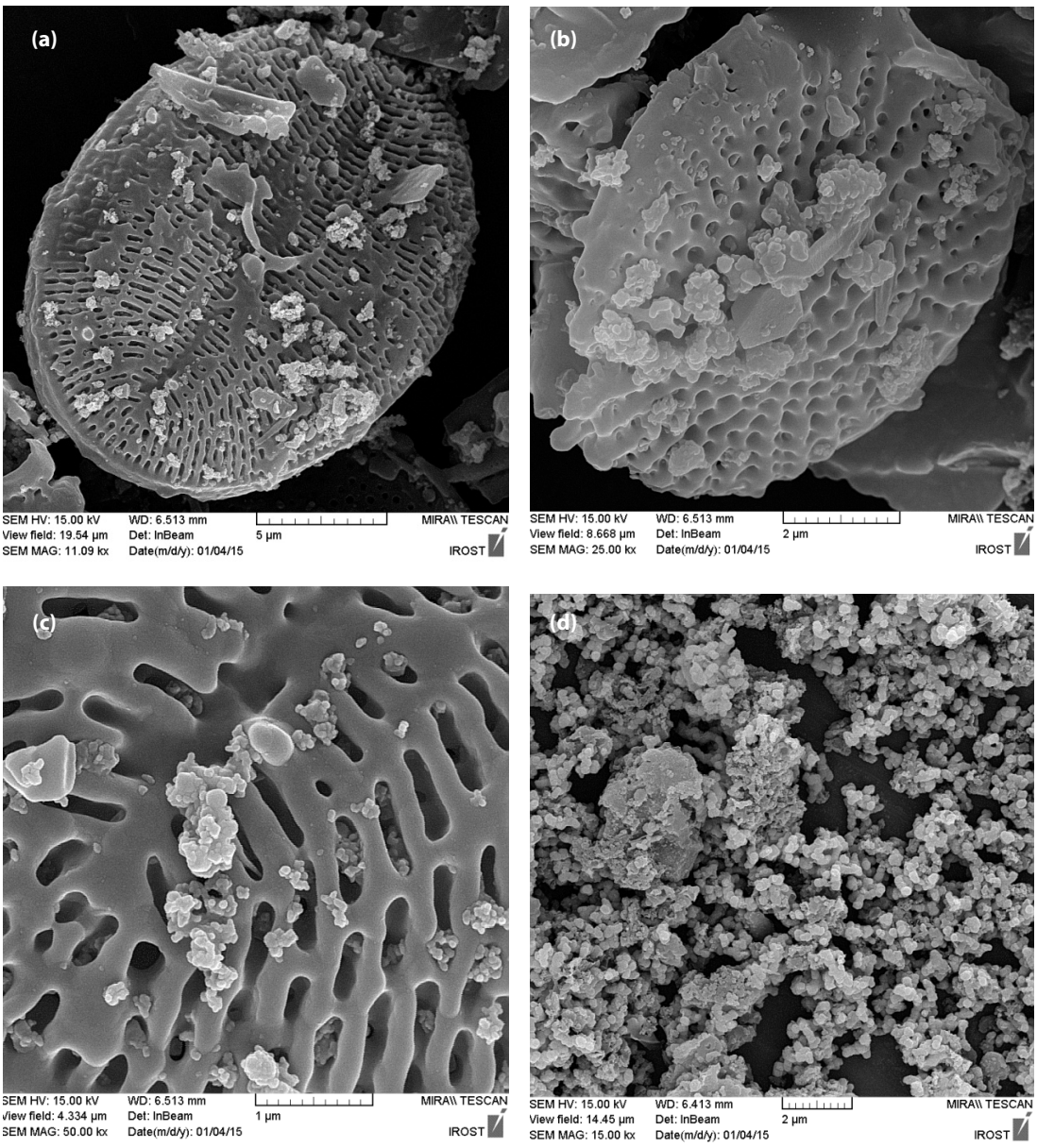

Fig. 2. FESEM of raw diatomite (a, b, and c) and Fe_2O_3/diatomite (d).

Table 3
Identification of IR adsorption band to specific vibrations [12]

Wavenumber (cm^{-1})	Vibrations
3,435	O–H stretching of water
1,635	H_2O bending
1,099 and 1,030	Si–O–Si stretching
798 and 780	Intertetrahedral Si–O–Si bending
695 and 470	O–Si–O bending
533	Si–O–Al bending

Therefore, the adsorption data were fitted to four kinetic models including pseudo-first-order (Eq. (2)), pseudo second order (Eq. (3)), Bangham (Eq. (4)), and intraparticle diffusion (Eq. (5)) (see Table 1).

Plots of kinetic study for the adsorption of NO_3^- onto Fe_2O_3/diatomite and calculated parameters for each are presented in Fig. 9 and Table 3, respectively. According to Fig. 9(b), the adsorption data are well represented by pseudo-second-order model. The higher value of R^2 (0.995) and closer calculated equilibrium capacities ($q_{e,cal}$) and experimental equilibrium capacity ($q_{e,exp}$) values confirmed that NO_3^- adsorption onto the Fe_2O_3/diatomite fitted the pseudo-second-order kinetic model, and chemisorption might be in control of the adsorption process [26]. Similar results were also obtained for the adsorption kinetics of various pollutants onto activated carbon cloth [27–30], sepiolite [31], vermiculite [32], and carbon nanotube [33].

Boundary layer diffusion (external mass transfer) and intraparticle diffusion (mass transfer through the pores) are two limiting steps in the ion-exchange process [34].

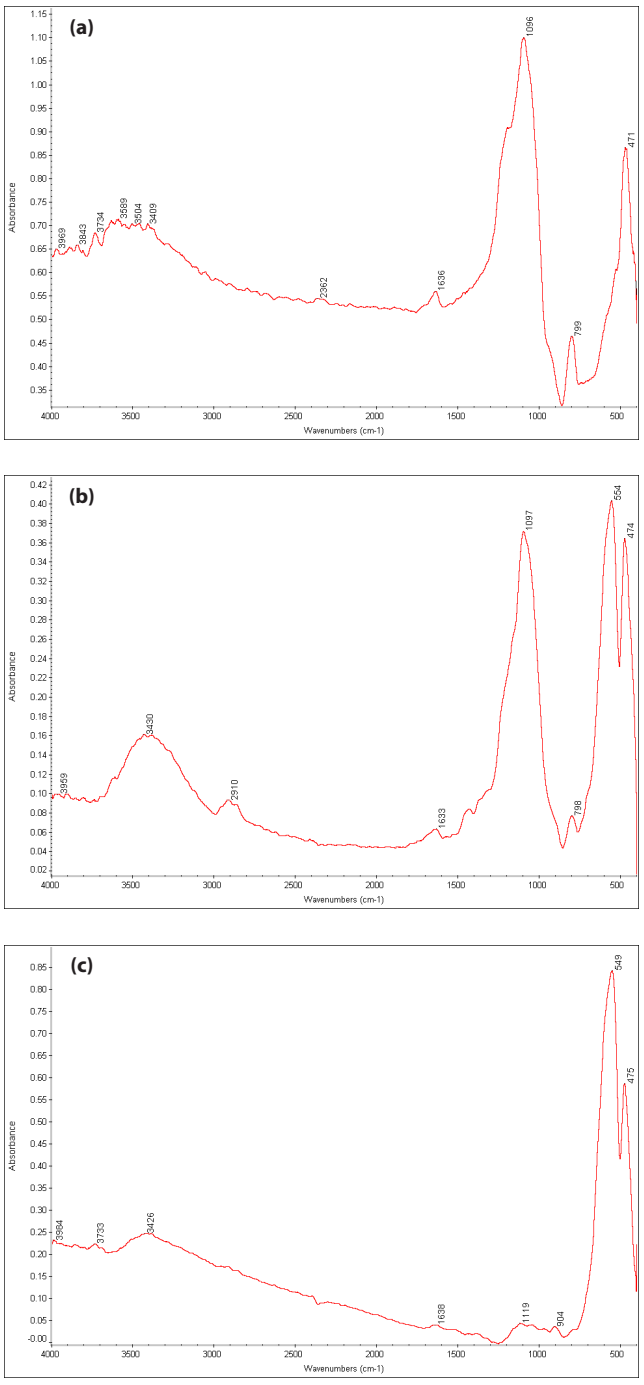

Fig. 3. FTIR spectra of: (a) raw diatomite, (b) Fe_2O_3/diatomite before adsorption, and (c) Fe_2O_3/diatomite after adsorption.

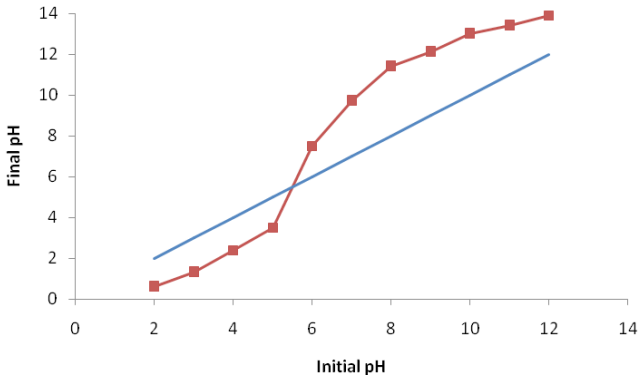

Fig. 4. Determination of pH_{zpc} using pH drift method.

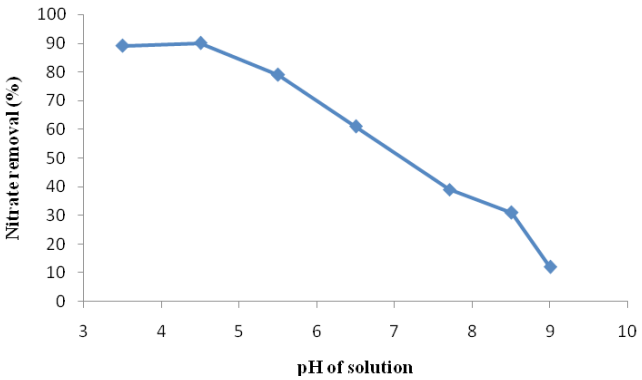

Fig. 5. Effect of pH solution on nitrate adsorption onto the adsorbent (initial nitrate concentration: 20 mg/L, adsorbent dose: 5 g/L, contact time: 100 min, temperature: 25°C).

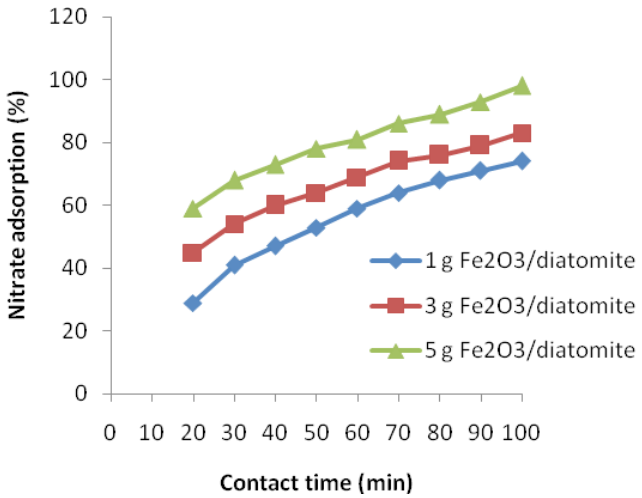

Fig. 6. Effect of adsorbent dose on nitrate adsorption as a function of contact time (conditions: initial nitrate concentration: 20 mg/L, pH: 4.5, temperature: 25°C).

The Bangham plot did not show any straight line indicating both pore, and boundary layer diffusions limit the adsorption process [35]. K_0 and α in this model are represented in Table 5.

Fig. 9(d) shows that the resulted curve for intraparticle diffusion is not linear over the studied time range and includes three portions. According to this plot, the both surface adsorption and intraparticle diffusion took part in the adsorption of NO_3^- on the Fe_2O_3/diatomite. Boundary layer diffusion is responsible for the first portion of this plot; in where, NO_3^- ions in solution diffuse to the external surface of the Fe_2O_3/diatomite. Rate-limiting behavior of intraparticle diffusion may be observed from the second portion of the plot, where slow adsorption of NO_3^- ions took place. The slope and intercept of this portion were used to derive K_i and C for

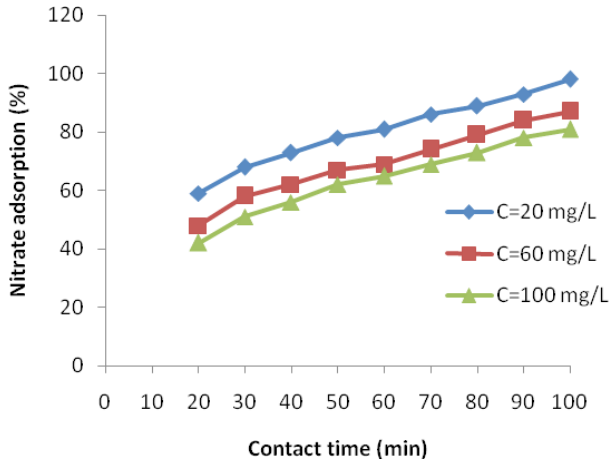

Fig. 7. Effect of initial nitrate concentration on nitrate removal as a function of contact time (conditions: adsorbent dose: 5 g/L, pH: 4.5, temperature: 25°C).

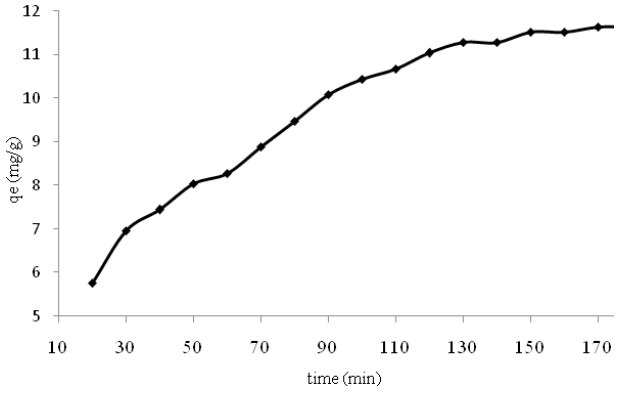

Fig. 8. Variations of adsorbed nitrate concentration vs. time, pH = 4.5, adsorbent dose = 5 g/L, nitrate concentration = 60 mg/L, contact time = 200 min.

intraparticle diffusion and boundary layer diffusion, respectively (Table 4). Final equilibrium was in the third portion, where the reduction of intraparticle diffusion occurred due to reduction in NO_3^- ions concentration in the solution.

3.8. Isotherm studies

Adsorption isotherms should also be determined in designing adsorption systems [25]. In the present study, three isotherm models including Langmuir, Freundlich, and D–R were used to study the relationship between adsorbed NO_3^- ions on the adsorbent (q_e) and unadsorbed NO_3^- ions in the solution (C_e) at equilibrium. Fig. 10 shows linear plots of the Langmuir, Freundlich, and D–R isotherms. The calculated parameters obtained from each isotherm model are presented in Table 5.

The R^2 values presented in Table 5 indicate that the Freundlich isotherm fitted the adsorption data well (R^2 = 0.993). This isotherm predicts that a non-monolayer adsorption of NO_3^- occurs on heterogeneous surface of the Fe_2O_3/diatomite [36,37]. The obtained value of n is greater than 1, which means a favorable adsorption process [25]

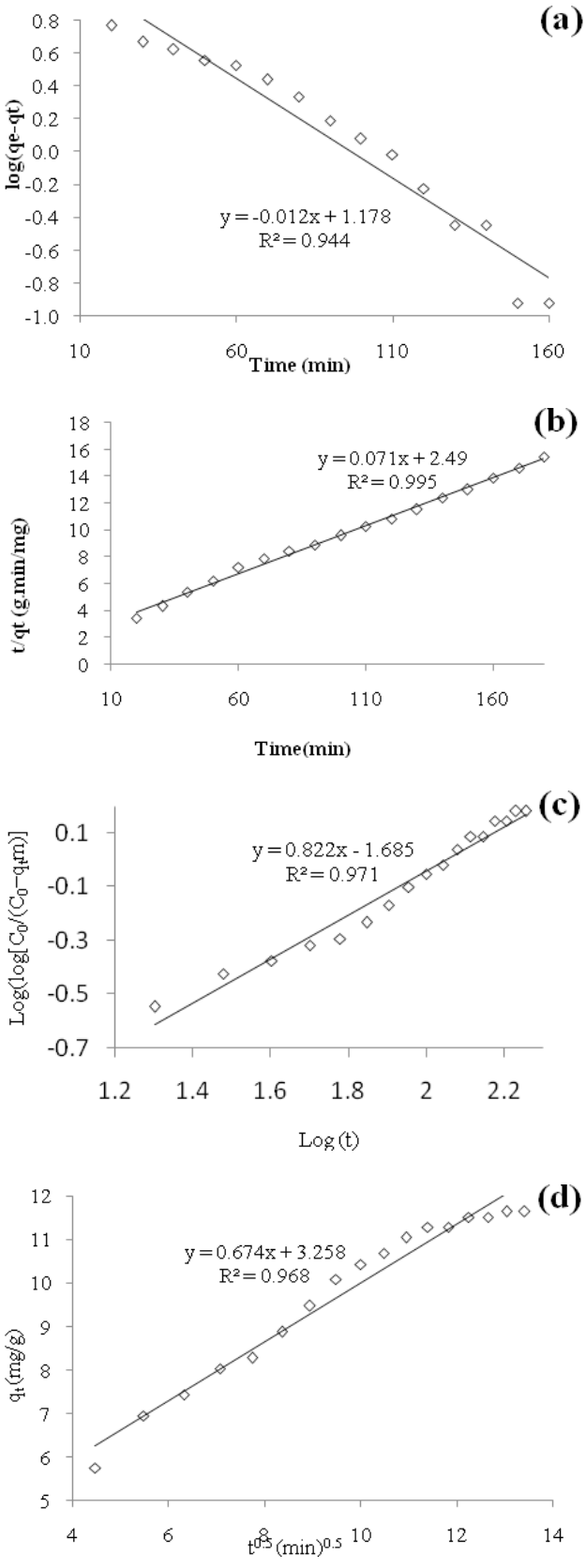

Fig. 9. Kinetic plots of NO_3^- adsorption onto Fe_2O_3/diatomite described by: (a) pseudo first order model, (b) pseudo second order model, (c) Bangham, and (d) intraparticle diffusion.

Table 4
Kinetic model parameters for the adsorption of NO_3^- using Fe_2O_3/diatomite adsorbent

Kinetic models	Kinetic parameters value	
Pseudo-first-order	k_1 (L.g^{-1})	0.028
	$q_{e,cal}$ (mg.g^{-1})	15.09
	$q_{e,exp}$ (mg.g^{-1})	11.64
	R^2	0.944
Pseudo-second-order	k_2 (g.mg^{-1}.min^{-1})	0.002
	$q_{e,cal}$ (mg.g^{-1})	14.02
	$q_{e,exp}$ (mg.g^{-1})	11.64
	R^2	0.995
Bangham	α	0.823
	K_0	0.971
	R^2	0.971
Intraparticle diffusion	k_i (mg.g^{-1}.min$^{-0.5}$)	0.627
	C	4.140
	R^2	0.968

Other researchers have also reported Freundlich as the suitable isotherm model for their data [38].

D–R isotherm model was also used to determine the physical or chemical nature of the NO_3^- adsorption on the Fe_2O_3/diatomite (see Fig. 2(c)). Table 5 represents the calculated values of D–R parameters. The R^2 value of 0.983 indicates that the D–R isotherm model also adequately fits to the equilibrium data for NO_3^-.

The mean free energy (E) using D–R isotherm may be calculated via Eq. (9) [26]:

$$E = 1/(-2\beta)^{0.5} \quad (2)$$

In fact, E describes the adsorption mechanism as follows: E values between 8 and 16 kJ/mol express that the adsorption process is chemical ion exchange; E values less than 8 kJ/mol indicate that the process is physical in nature; and E values above 16 kJ/mol imply that the process is chemisorptions [39]. In the present study, E was found to be 12.91 kJ/mol, indicating that the adsorption of NO_3^- ions is chemical ion exchange.

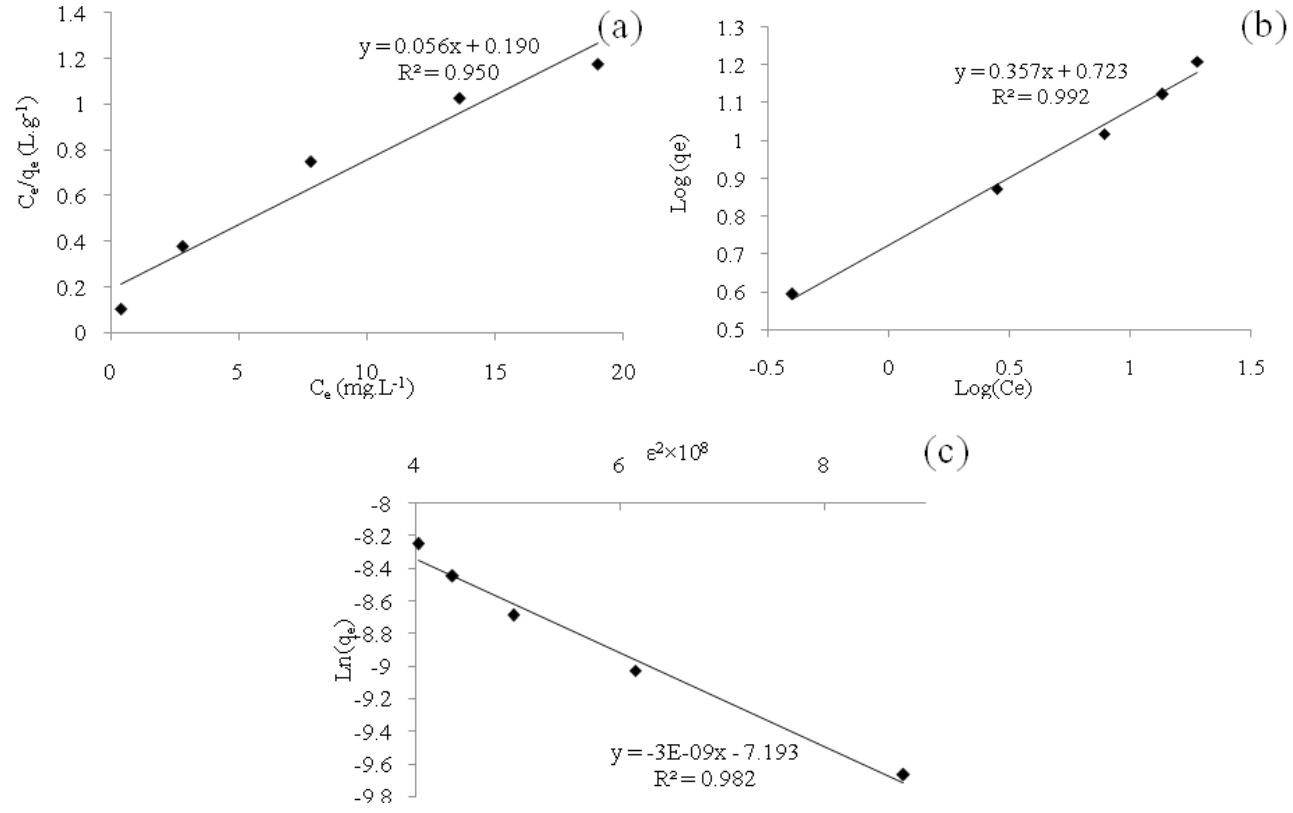

Fig. 10. Equilibrium isotherm analysis for adsorption of NO_3^- using Fe_2O_3/diatomite: (a) Langmuir, (b) Freundlich, and (c) D–R models.

Table 5
Isotherm model parameters for adsorption of NO_3^- using Fe_2O_3/diatomite

Langmuir isotherm			Freundlich isotherm			D–R isotherm		
q_m (mg.g^{-1})	K_L (L/mg)	R^2	n	K_F (mg$^{(1-1/n)}$).(L$^{1/n}$.g^{-1})	R^2	q_m (mol.g^{-1})	β	R^2
17.67	0.297	0.951	2.800	5.293	0.993	7.5×10^{-4}	-3×10^{-9}	0.983

4. Conclusions

The adsorption of nitrate from aqueous solution using diatomite-supported ferric oxide nanoparticle under different operational conditions was investigated. The adsorbent was prepared by simple WIM. The modification of diatomite using ferric oxide nanoparticles was effective for nitrate adsorption. The variation of adsorption performance of diatomite-supported ferric oxide nanoparticles for nitrate adsorption exhibited nitrate adsorption of 93% at a solution pH of 4.5 with 5 g/L Fe_2O_3/diatomite content. The kinetic and isotherm models were well represented by pseudo-second-order model and Freundlich, respectively. Based on the experimental results of the present study, Fe_2O_3/diatomite can be recommended as a cost-effective adsorbent for nitrate removal from aqueous media.

Acknowledgment

The authors would like to express sincere appreciation to the Kurdistan University of Medical Sciences.

References

[1] M. Dore, P. Simon, A. Deguin, J. Vicot, Removal of nitrate in drinking water by ion-exchange-impact on the chemical quality of treated water, Water. Res., 20 (1986) 221–232.
[2] K. Salem, J. Sandeaux, J. Molenat, R. Sandaeaux, C. Gavach, Elimination of nitrate from drinking water by electrochemical membrane processes, Desalination, 101 (1995) 123–131.
[3] F. Hell, J. Lahnteiner, H. Frischherz, G. Baumgartner, Experience with full-scale electrodialysis for nitrate and hardness removal, Desalination, 117 (1998) 173–180.
[4] K. Ismail, Effect of operating conditions on the separation of ammonium and nitrate ions with nanofiltration and reverse osmosis membranes, J. Environ. Sci. Health., Part A, 37 (2002) 1347–1359.
[5] S. Dehestaniathar, A. Rezaee, Adsorption of nitrate from aqueous solution using activated carbon-supported Fe_0, $Fe_2(SO_4)_3$, and $FeSO_4$, J. Adv. Environ. Health Res., 2 (2014) 181–188.
[6] P. Mishra, R. Patel, Use of agricultural waste for the removal of nitrate-nitrogen from aqueous medium, J. Environ. Manage., 90 (2009) 519–522.
[7] C. Mena-Duran, M. Sun Kou, T. Lopez, J. Azamar-Barrios, D. Aguilar, M. Domínguez, Nitrate removal using natural clays modified by acid thermoactivation, Appl. Surf. Sci., 253 (2007) 5762–5766.
[8] M.C. Bruzzoniti, R.M. De Carlo, C. Sarzanin, D. Caldarola, B. Onida, Novel insights in Al-MCM-41 precursor as adsorbent for regulated haloacetic acids and nitrate from water, Environ. Sci., Pollut. Res. Int., 19 (2012) 4176–4183.
[9] K. Mizuta, T. Matsumoto, Y. Hatate, K. Nishihara, T. Nakanishi, Removal of nitrate-nitrogen from drinking water using bamboo powder charcoal, Bioresour. Technol., 95 (2004) 255–257.
[10] N. Agyei, C. Strydom, J. Potgieter, The removal of phosphate ions from aqueous solution by fly ash, slag, ordinary Portland cement and related blends, Cement Concrete Res., 32 (2002) 1889–1897.
[11] R. Gaikwad, A. Warade, Removal of nitrate from groundwater by using natural zeolite of Nizarneshwar Hills of Western India, J. Water Resour. Hydraul. Eng., 3 (2014) 74–80.
[12] A. Chaisena, K. Rangsriwatananon, Effects of thermal and acid treatments on some physico-chemical properties of lampang diatomite, Suranaree J. Sci. Technol., 11 (2004) 289–299.
[13] M. Aivalioti, P. Papoulias, A. Kousaiti, E. Gidarakos, Adsorption of BTEX, MTBE and TAME on natural and modified diatomite, J. Hazard. Mater., 207 (2012) 117–127.
[14] G. Yang, H. Lee, Chemical reduction of nitrate by nanosized iron: kinetics and pathways, Water. Res., 39 (2005) 884–894.
[15] C. Luiz, R. VRA, D. Riosa, K. Vijayendra, M. Rochel, Clay–iron oxide magnetic composites for the adsorption of contaminants in water, Appl. Clay. Sci., 22 (2013) 169–177.
[16] M. Al-Ghouti, Y. Al-Degs, A. Khraisheh, M. Ahmad, S. Allen, Mechanisms and chemistry of dye adsorption on manganese oxides-modified diatomite, J. Environ. Manage., 90 (2009) 3520–3527.
[17] M. Al-Ghouti, M. Khraisheh, M. Tutunji, Flow injection potentiometric stripping analysis for study of adsorption of heavy metal ions onto modified diatomite, Chem. Eng. J., 104 (2004) 83–91.
[18] G. Sheng, S. Wang, J. Hu, Y. Lu, J. Li, Y. Dong, X. Wang, Adsorption of Pb(II) on diatomite as affected via aqueous solution chemistry and temperature, Colloids Surf. A, 339 (2209) 159–166.
[19] M. Pantoja, H. Jones, H. Garelick, H. Mohamedbakr, M. Burkitbayev, The removal of arsenate from water using iron-modified diatomite (D-Fe): isotherm and column experiments, Environ. Sci. Pollut. Res., 21 (2014) 495–506.
[20] N. Caliskan, R. Kul, S. Alkan, G. Sogut, I. Alacabey, Adsorption of zinc(II) on diatomite and manganese-oxidemodified diatomite: a kinetic and equilibrium study, J. Hazard. Mater., 193 (2011) 27–36.
[21] S. Dehestaniathar, M. Khajelakzay, M. Ramezani-Farani, H. Ijadpanah-Saravi, Modified diatomite-supported CuO–TiO_2 composite: preparation, characterization and catalytic CO oxidation, J. Taiwan Inst. Chem. Eng., 58 (2016) 252–258.
[22] APHA, AWWA, WEF, Standard Methods for the Examination of Water and Wastewater, 20th ed., APHA, AWWA, WEF, Washington, D.C., USA 1998, pp. 770–773.
[23] G. Newcombe, R. Hayes, M. Drikas, Granular activated carbon: importance of surface properties in the adsorption of naturally occurring organics, Colloids Surf., A, 78 (1993) 65–71.
[24] B. Hadjar, M. Hamdi, J. Jaber, Z. Brendle, H. Kessaissia, J. Balard, B. Donnet, Elaboration and characterisation of new mesoporous materials from diatomite and charcoal, Microporous Mesoporous Mater., 107 (2007) 219–226.
[25] N. Dizge, B. Keskinler, H. Barlas, Sorption of Ni(II) ions from aqueous solution by Lewatit cation-exchange resin, J. Hazard. Mater., 167 (2009) 915–926.
[26] P. Teymouri, M. Ahmadi, A.A. Babaei, K. Ahmadi, N. Jaafarzadeh, Biosorption studies on NaCl-modified ceratophyllum demersum: removal of toxic chromium from aqueous solution, Chem. Eng. Commun., 200 (2013) 1394–1413.
[27] E. Ayranci, O. Duman, Structural effects on the interactions of benzene and naphthalene sulfonates with activated carbon cloth during adsorption from aqueous solutions, Chem. Eng. J., 156 (2010) 70–76.
[28] O. Duman, E. Ayranci, Attachment of benzo-crown ethers onto activated carbon cloth to enhance the removal of chromium, cobalt and nickel ions from aqueous solutions by adsorption, J. Hazard. Mater., 176 (2010) 231–238.
[29] E. Ayranci, O. Duman, In-situ UV-visible spectroscopic study on the adsorption of some dyes onto activated carbon cloth, Sep. Sci., Technol., 44 (2009) 3735–3752.
[30] O. Duman, E. Ayranci, Adsorptive removal of cationic surfactants from aqueous solutions onto high-area activated carbon cloth monitored by in situ UV spectroscopy, J. Hazard. Mater., 174 (2010) 359–367.
[31] O. Duman, S. Tunç, T. Polat, Adsorptive removal of triarylmethane dye (Basic Red 9) from aqueous solution by sepiolite as effective and low-cost adsorbent, Microporous Mesoporous Mater., 210 (2015) 176–184.
[32] O. Duman, S. Tunç, T. Polat, Determination of adsorptive properties of expanded vermiculite for the removal of C. I. Basic Red 9 from aqueous solution: kinetic, isotherm and thermodynamic studies, Appl. Clay Sci., 109–110 (2015) 22–32.
[33] O. Duman, S. Tunç, T. Polat, B. Bozoğlan, Synthesis of magnetic oxidized multiwalled carbon nanotube-κ-carrageenan-Fe_3O_4 nanocomposite adsorbent and its application in cationic Methylene Blue dye adsorption, Carbohydr. Polym., 147 (2016) 79–88.

[34] N. Jaafarzadeh, P. Teymouri, A.A. Babaei, N. Alavi, M. Ahmadi, Biosorption of cadmium (II) from aqueous solution by NaCl-treated ceratophyllum demersum, Environ. Eng. Manag. J., 13 (2014) 763–773.
[35] Z. Belala, M. Jeguirim, M. Belhachemi, F. Addoun, G. Trouvé, Biosorption of basic dye from aqueous solutions by Date Stones and Palm-Trees Waste: kinetic, equilibrium and thermodynamic studies, Desalination, 271 (2011) 80–87.
[36] Y. Ren, H.A. Abbood, F. He, H. Peng, K. Huang, Magnetic EDTA-modified chitosan/SiO_2/Fe_3O_4 adsorbent: preparation, characterization, and application in heavy metal adsorption, Chem. Eng. J., 226 (2013) 300–311.
[37] R. Darvishi Cheshmeh Soltani, A. Rezaee, G. Shams Khorramabadi, K. Yaghmaeian, Optimization of lead(II) biosorption in an aqueous solution using chemically modified aerobic digested sludge, Water Sci. Technol., 63 (2011) 129–135.
[38] C. Namasivayam, D. Sangeetha, Removal and recovery of Nitrate from water by $ZnCl_2$ activated carbon from coconut coir pith, and agricultural solid waste, Indian J. Chem. Technol., 12 (2005) 513–521.
[39] M.A. Mahmoud, Kinetics and thermodynamics of aluminum oxide nanopowder as adsorbent for Fe (III) from aqueous solution, Beni-Seuf Univ. J. Appl. Sci., 4 (2015) 142–149.